2002

# Compact Methods for Measuring Stress Birefringence

Nathan A. Hagen, Derek S. Sabatke, James F. Scholl, Peter A. Jansson, Weinong W. Chen[a], Eustace L. Dereniak, David T. Sass[b]

Optical Sciences Center, University of Arizona, Tucson, AZ 85721
[a]Dept of Aerospace and Mechanical Engineering, University of Arizona, Tucson, AZ 85721
[b]U. S. Army TACOM, Warren, MI 48397

## ABSTRACT

The recent development of channelled spectropolarimetry presents opportunities for spectropolarimetric measurements of dynamic phenomena in a very compact instrument. We present measurements of stress-induced birefringence in a simple plastic by both a reference rotating-compensator spectropolarimeter and a channelled spectropolarimeter. The agreement between the two instruments shows the promise of the channelled technique and provides a proof-of-principle that the method can be used for a very simple conversion of imaging spectrometers into imaging spectropolarimeters.

**Keywords:** polarimetry, spectropolarimetry, birefringence, photoelasticity

## 1. INTRODUCTION

The need to measure retardance accurately is common in optical systems, and the many different techniques employed each offer their own unique strengths and weaknesses, with the requirements of a given application informing the suitability of the polarimeter design. For reliability and accuracy, a common choice is to use a "time-sequential" instrument with rotating polarization elements.[1] For high-speed polarimetry, electro-optic or photoelastic modulators are often used in place of a rotating element.[2] For instantaneous acquisition of polarization information, division-of-aperture[3] or division-of-amplitude[4] designs are often employed. The technique of channelled spectropolarimetry,[5] while not widely known, offers advantages of its own and is well suited to measurements of the wavelength-dependence of birefringence. Photoelasticity applications can benefit substantially from obtaining spectral information,[6] and we present a method which uses the derived birefringence to avoid some of the ambiguities of photoelastic fringe analysis.

## 2. CHANNELLED SPECTROPOLARIMETRY

The hardware configuration of a channelled spectropolarimeter (CHSP), illustrated below in Fig. 1, comprises two thick retarders, $\boldsymbol{R}_1$ and $\boldsymbol{R}_2$, oriented respectively at 0° and 45° to horizontal, followed by an analyzer $\boldsymbol{A}$ and the spectrometer. The electric field of light passing through the system can be most conveniently represented in terms of the Stokes vector representation

$$\boldsymbol{s} = \begin{pmatrix} s_0 \\ s_1 \\ s_2 \\ s_3 \end{pmatrix} = \begin{pmatrix} I_{total} \\ I_0 - I_{90} \\ I_{45} - I_{-45} \\ I_{rc} - I_{lc} \end{pmatrix} = \begin{pmatrix} E_x E_x^* + E_y E_y^* \\ E_x E_x^* - E_y E_y^* \\ E_x^* E_y + E_x E_y^* \\ i(E_x^* E_y - E_x E_y^*) \end{pmatrix}, \tag{1}$$

where each of the three polarization components ($s_1$, $s_2$, $s_3$) are intensities given by differences in orthogonal elements of the beam. Using Mueller calculus, we can then calculate the spectral polarization state of the beam by cascading Mueller matrices for each optical element. Using $\boldsymbol{A}(\phi)$ to represent a linear analyzer oriented at

Further author information: (Send correspondence to E.L.D.) E-mail: eustace@u.arizona.edu

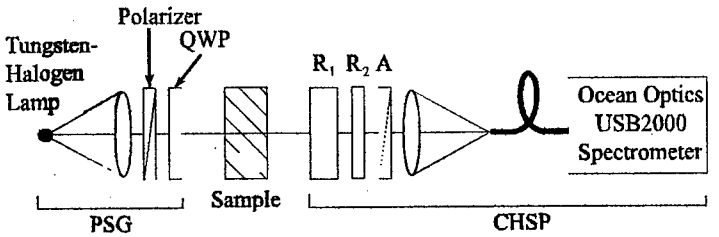


**Figure 1.** A diagram of the experimental layout, using a broad spectrum polarization state generator (PSG), the sample, and a channelled spectropolarimeter (CHSP).

angle $\phi$ to the horizontal, and $\boldsymbol{R}(\phi,\delta)$ for a linear retarder oriented at angle $\phi$ with retardance $\delta$, then the Mueller-calculus of the system will take an input polarization state $\boldsymbol{s}_{in}$ and produce an output (before the spectrometer) of

$$\boldsymbol{s}_{out} = \boldsymbol{A}(0)\cdot\boldsymbol{R}(\tfrac{\pi}{4},\delta_2)\cdot\boldsymbol{R}(0,\delta_1)\cdot\boldsymbol{s}_{in} = 1/2\begin{pmatrix} s_0 + s_1\cos(\delta_2) + s_2\sin(\delta_1)\sin(\delta_2) - s_3\cos(\delta_1)\sin(\delta_2) \\ s_0 + s_1\cos(\delta_2) + s_2\sin(\delta_1)\sin(\delta_2) - s_3\cos(\delta_1)\sin(\delta_2) \\ 0 \\ 0 \end{pmatrix} . \quad (2)$$

The detector itself is directly sensitive only to the total intensity-component ($s_0$) of the Stokes vector, and thus acts as a device with a Mueller matrix of (1 0 0 0). Multiplying the above output Stokes vector with the detector sensitivity matrix gives an output of the form

$$2P(\sigma) = s_0 + s_1\cos(\delta_2) + s_2\sin(\delta_1)\sin(\delta_2) - s_3\cos(\delta_1)\sin(\delta_2) . \quad (3)$$

From this result, we can see that the four Stokes components are each encoded as sinusoidal modulations in the intensity spectrum reaching the detector; and, since the retardances $\delta_1$ and $\delta_2$ are both wavenumber-dependent, the encoded power spectrum itself is wavenumber-dependent (see Figs 2&3 for examples of the unencoded and encoded spectra). Rewriting the above equation in terms of complex exponentials, we can gather terms with like carrier terms, giving the result:

$$\begin{aligned} P(\sigma) \;=\; & \tfrac{1}{2}s_0 + \tfrac{1}{4}s_1(e^{i\delta_2} + e^{-i\delta_2}) \\ & + \tfrac{1}{8}[(s_2 - is_3)e^{i(\delta_2+\delta_1)} + (s_2 + is_3)e^{-i(\delta_2+\delta_1)} + (-s_2 - is_3)e^{i(\delta_2-\delta_1)} + (-s_2 + is_3)e^{-i(\delta_2-\delta_1)}] , \end{aligned} \quad (4)$$

recalling that $s_1, s_2, s_3, \delta_1$, and $\delta_2$ are *all* functions of wavenumber $\sigma$. The seven terms in the equation above represent the seven "channels" into which the polarization information is encoded. If we now take the autocorrelation function (Inverse Fourier Transform) of this power spectrum, we can then see the resulting 7-channel distribution, shown in Figs 4&5.

Before discussing how to reconstruct the Stokes spectra from the autocorrelation function, it is first useful to have a concrete idea of the meaning of the function's abscissa. If we first consider the case of input light polarized along the horizontal axis, then we can note that this light will be unaffected (other than by an absolute phase) by $\boldsymbol{R}_1$, whose fast axis is aligned to the horizontal. As this light passes into the $\boldsymbol{R}_2$, however, it will be separated equally into two orthogonal elements, one aligned along $\boldsymbol{R}_2$'s fast axis and the other along its slow axis, such that the two components of the originally horizontally-polarized beam will experience a relative path difference equal to $\boldsymbol{R}_2$'s retardance. As this light passes through the analyzer it will experience an attenuation dependent upon the polarization angle, and since the retardance is heavily wavelength-dependent in a thick retarder, this polarization angle will vary rapidly with wavenumber, creating a sinusoidally-varying attenuation of the transmitted beam with respect to wavenumber. Thus, the abscissa of the autocorrelation function readily appears as the optical path difference experienced by the two orthogonal elements comprising each individual Stokes component (*i.e.*$I_0$ and $I_{90}$ in the case of $s_1$).

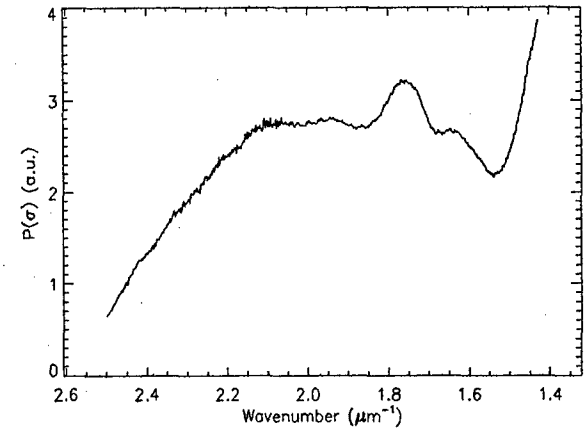


**Figure 2.** The measured channelled spectrum for an unpolarized input.

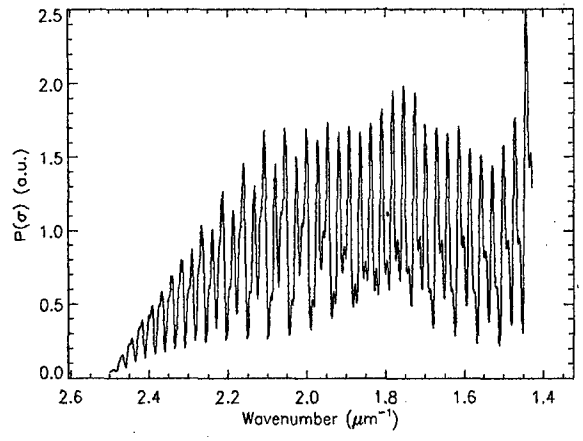


**Figure 3.** The measured channelled spectrum for a complex input polarization state.

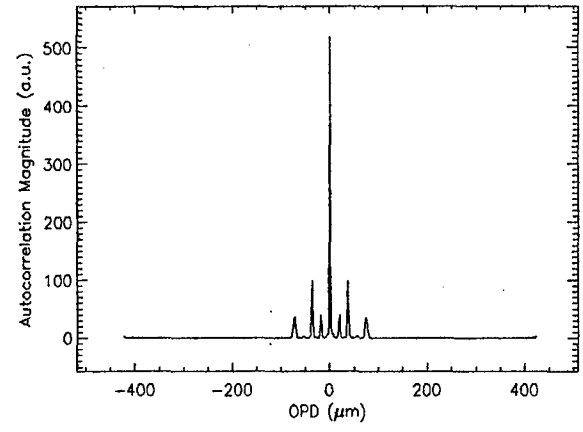


**Figure 4.** The magnitude of the channelled spectrum autocorrelation function for a complex input polarization state.

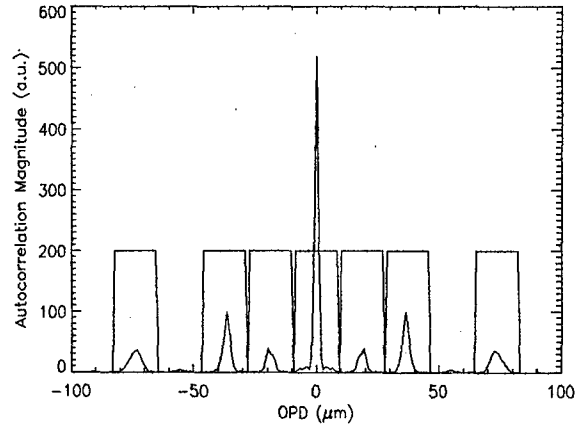


**Figure 5.** Magnification of the central region of Fig. 5, with Fourier windows superimposed (and rescaled for visibility).

The prototype instrument for these measurements uses a pair of retarders whose thickness ratio is 3:1, producing the distribution of bands in the autocorrelation function as shown in Fig. 5. It is known that a thickness ratio of 1:2 actually provides a more efficient use of the spectral bandwidth,[7] lacking the wasted region between bands, yet the configuration in use here is still functional. Additionally, the spectrometer chosen for the instrument provides a wavelength resolution which is considerably finer than the modulations introduced into the encoded spectrum, resulting in some wasted bandwidth at the outer portions of the autocorrelation function which are apparent in Fig. 4. An upgrade of the prototype will involve use of thicker retarders with the ideal thickness ratio.

With each of the Stokes components separated in the OPD-domain, we can then mask off a given component with a Fourier windowing function and inverse transform to derive its distribution in the spectral domain (a "Stokes spectrum"). A result of the use of Fast Fourier Transform routines in the reconstruction is the creation of artifacts at both the low-$\lambda$ and high-$\lambda$ ends of the spectral region. By proper selection of the Fourier windowing function, these artifacts can be restricted to the edge region such that truncation will result in a minimal loss of data.

## 3. ROTATING-COMPENSATOR SPECTROPOLARIMETRY

As a reference against which to compare the prototype CHSP instrument, we constructed a standard polarimeter design which we refer to as a rotating-compensator spectropolarimeter (RCSP), consisting of a rotating quarter-wave plate (oriented at various angles $\phi$), followed by an analyzer and spectrometer. Mueller calculus for this kind of system gives the form of light reaching the detector as

$$\begin{aligned} \boldsymbol{s}_{out} &= \boldsymbol{A}(0) \cdot \boldsymbol{R}(\phi, \delta) \cdot \boldsymbol{s}_{in} \qquad (5) \\ &= 1/2 \begin{pmatrix} s_0 + s_1[\cos^2(2\phi) + \sin^2(2\phi)\cos\delta] + s_2[\sin(2\phi)\cos(2\phi)(1-\cos\delta)] - s_3[\sin(2\phi)\sin\delta] \\ s_0 + s_1[\cos^2(2\phi) + \sin^2(2\phi)\cos\delta] + s_2[\sin(2\phi)\cos(2\phi)(1-\cos\delta)] - s_3[\sin(2\phi)\sin\delta] \\ 0 \\ 0 \end{pmatrix} . \end{aligned}$$

The detector output will thus take the form

$$2P(\sigma) = s_0 + s_1[\cos^2(2\phi) + \sin^2(2\phi)\cos\delta] + s_2[(1-\cos\delta)sin(2\phi)\cos(2\phi)] - s_3[\sin(2\phi)\sin\delta] . \qquad (6)$$

The retarder used, while nominally a quarter-wave achromat, has significant dispersion of retardation, and so $\delta$ is a function of wavenumber. The orientation of the fast axis $\phi$ also has a slight but significant wavelength dependence, so that both of the two retarder parameters had to be carefully calibrated to achieve accurate results. Rewriting the functional form of $P$ in terms of the orientation angles used and the intensities measured gives $\boldsymbol{P}(\phi) = \boldsymbol{W}(s, \phi) \cdot \boldsymbol{s}_{in}$, where $\boldsymbol{W}$ is the "system matrix" connecting measured intensities with the input Stokes components. Written out in full, this equation has the form

$$\begin{pmatrix} P(\phi_0) \\ P(\phi_1) \\ P(\phi_2) \\ P(\phi_3) \\ P(\phi_4) \end{pmatrix} = \begin{pmatrix} W(s_0,\phi_0) & W(s_1,\phi_0) & W(s_2,\phi_0) & W(s_3,\phi_0) \\ W(s_0,\phi_1) & W(s_1,\phi_1) & W(s_2,\phi_1) & W(s_3,\phi_1) \\ W(s_0,\phi_2) & W(s_1,\phi_2) & W(s_2,\phi_2) & W(s_3,\phi_2) \\ W(s_0,\phi_3) & W(s_1,\phi_3) & W(s_2,\phi_3) & W(s_3,\phi_3) \\ W(s_0,\phi_4) & W(s_1,\phi_4) & W(s_2,\phi_4) & W(s_3,\phi_4) \end{pmatrix} \cdot \begin{pmatrix} s_0 \\ s_1 \\ s_2 \\ s_3 \end{pmatrix} . \qquad (7)$$

In this form it is easy to see that the system matrix can be pseudo-inverted upon insertion of the known orientation angles and retardance.[8] Obtaining the pseudoinverse $\boldsymbol{W}^+$, we can multiply $\boldsymbol{W}^+$ into the above matrix equation giving $\boldsymbol{s}_{in} = \boldsymbol{W}^+(s, \phi) \cdot \boldsymbol{P}(\phi)$, our desired result. Performing this analysis at each wavelength allows the reconstruction of the full Stokes spectra. Although the RCSP analysis can be performed using Fourier techniques, we find the pseudoinverse method more straightforward when dealing with the wavelength-dependence of $\delta$ and $\phi$ in the waveplate.

Having our prototype and reference instruments, we can use the polarization state generator to send in known polarization states, and compare the fidelity of SOP reconstruction. Fig. 6 shows two such comparisons, from which several features are noticeable: (1) the edge artifacts in the CHSP reconstruction can be entirely eliminated by truncating the spectral region of interest from 400–700 nm to 415–685 nm. (2) While the reconstructions of 90° LP show excellent agreement, there is a substantial discrepancy in that for RCP, which we suspect to be due to digitization effects and aliasing resulting from the use of only a minor portion of the total available spectral bandwidth.

## 4. MEASURING RETARDANCE

To evaluate the performance of each polarimeter, we can now generate a spectrum with a known SOP, pass it through a sample, and measure the output SOP. To perform a linear retardance measurement for the two polarimeter instruments we present here, it is ideal to use a broad-spectrum source which outputs circularly-polarized collimated light. Into this beam we place the birefringent material at normal incidence. The spectropolarimeter is then placed to measure the output SOP across the entire wavelength region of interest (in this case 415–685 nm).

In the Poincaré Sphere representation of the Stokes vector, the action of a linear retarder on the input Stokes vector is to rotate it by an angle $\delta$ (the magnitude of the retardation in radians) where the axis of rotation is

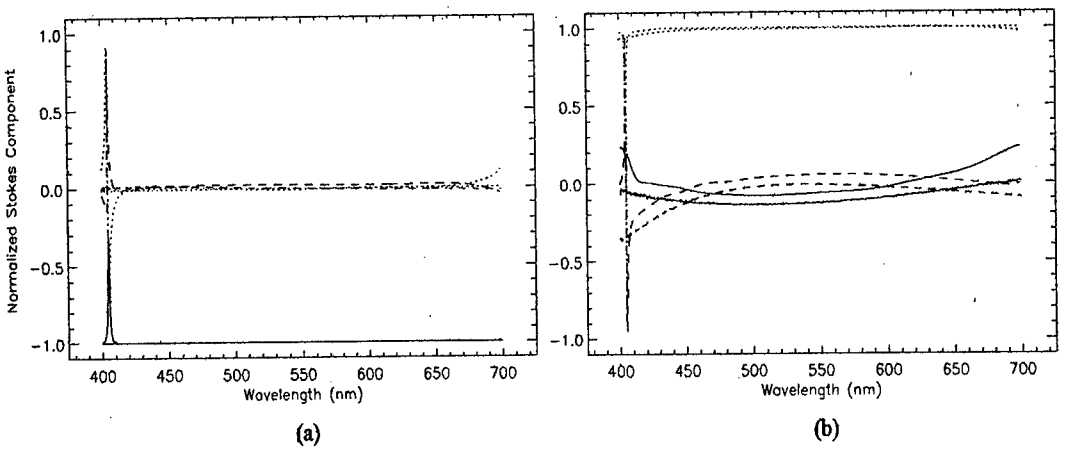


**Figure 6.** RCSP and CHSP reconstructions for (a) horizontally-polarized input, and (b) RCP input ($s_1$ = solid, $s_2$ = dashed, $s_3$ = dotted). The edge artifacts appear only in the CHSP data.

twice the orientation angle $\phi$ of the waveplate fast axis with respect to horizontal. Since the retardation of a birefringent material is in general wavelength-dependent, the result will be a "Stokes snake" strung across the surface of the Poincaré Sphere. (For an illustration of this, see Fig. 7.) So far, our analysis does not yet include the effect of multiple-reflections inside the sample, which can cause a modulation in the retardation curve with respect to wavelength.[9]

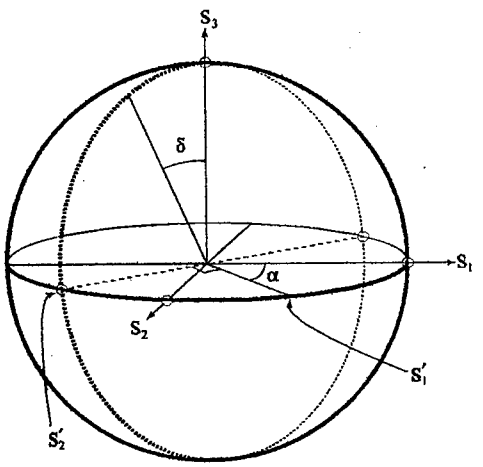


**Figure 7.** Representation on the Poincaré Sphere, showing the locus of points on the great circle generated by a retarder oriented at angle $\phi$ on an RCP input.

The projection of the Stokes snake onto the Poincaré Equator (the $s_1$-$s_2$ plane) produces a linear distribution of Stokes vectors at right angles to the azimuthal ($\alpha = 2\phi$) axis of the sample (shown figuratively in Fig. 7; actual measurements are shown in Fig. 8). A linear fit to this distribution allows us to establish the azimuthal angle $\alpha$ with respect to the $s_2$ axis. Half this angle is then the orientation angle $\phi$ of the fast axis of the retarder.

As the Stokes snake wraps around the surface of the Sphere, it traces out a circle. If the input polarization vector is circularly polarized (*i.e.* at one of the poles of the Sphere), then the trace is a great circle of the Sphere, which maximizes the information content. Knowing the azimuth angle from the step above, we can rotate the Poincaré Sphere about the $s_3$-axis such that the new coordinate system $(s_1', s_2', s_3)$ has its $s_1'$-axis coincident with

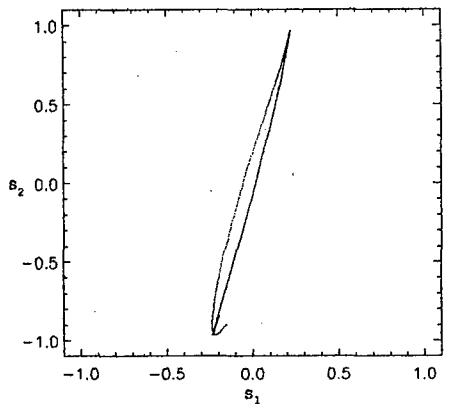


**Figure 8.** The "Stokes snake" projection onto the Poincaré Equator. The degree of deviation of the data shown from linear is more likely a property of the complex photoelastic response of the sample than a reconstruction artifact, as it shows up clearly in both instruments.

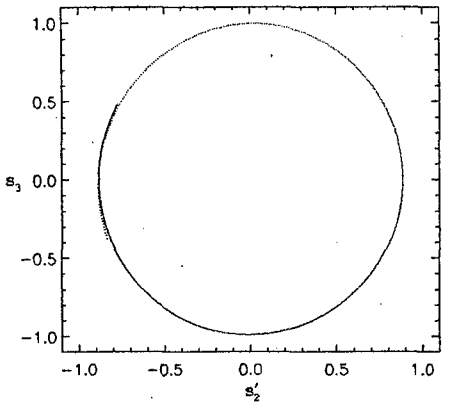


**Figure 9.** The circle on the Poincaré Sphere traced out by the input RCP Stokes spectrum passing through a linear retarder. $s_2'$ is the $s_2$ coordinate axis rotated through the azimuth angle $\alpha$.

the azimuthal angle $\alpha$. In this new coordinate system, we can then plot the data points on the $(s_2', s_3)$ plane, producing an arc which may be part of a circle, or perhaps a circle which overlaps itself (see Fig. 9). We can use the relation $tan(2\delta) = s_2'/s_3$ to determine the angle of each given vector and, knowing the input SOP, we have the relative retardation $\delta$, folded by modulo $2\pi$. In order to determine the *absolute* retardation, we need to supply a missing constant $n$ number of rotations.

The relation of retardance to wavenumber follows the relation $\delta(\sigma) = 2\pi d\,\Delta n\,\sigma$, where $d$ is the physical thickness of the retarder and $\Delta n$ is its birefringence. Here we have a linear equation in sigma implying that $\delta(\sigma) = 0$ when $\sigma = 0$, which provides the missing constant needed. This only holds true when $\Delta n$ is a constant, but, for materials which are transparent in the visible region, the assumption of a constant is not a bad one and the resulting model can produce good results. Having our retardance values, we can then measure the physical thickness of our sample to derive the birefringence, $\Delta n = \lambda\delta/2\pi d$

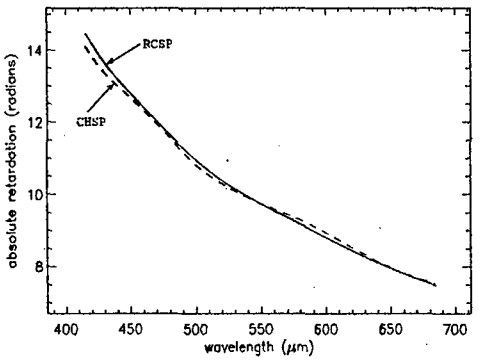


**Figure 10.** The reconstructed absolute retardance values for the sample.

For monochromatic polarimeters, multiple measurements are normally necessary to unambiguously determine the azimuthal axis of the sample under scrutiny, but gathering the polarization data over a wide spectrum eliminates the ambiguity. For the RCSP design, it is of course still necessary to acquire multiple measurements to obtain the Stokes snake, but the CHSP is able to acquire this information in a single snapshot. With the CHSP's acquisition time limited by the speed of the spectrometer, this technique is not necessarily *fast*, but

it does allow the instrument to capture dynamic phenomena on a substantially shorter timescale. Thus, while slower than many monochromatic techniques, the channelled spectropolarimeter's measurement's access to the orientation angle can provide a distinct advantage for some applications.

## 5. PHOTOELASTIC MODEL

For many isotropic materials, stresses applied to the material along a single axis alter it into a uniaxial one, where the induced birefringence axis coincides with that of the applied stress. Thus, photoelastic experiments are an instance of retardation measurement. In the real world, no material is completely isotropic, and its response to applied stress can be much more complex than assumed in this model; whereas some materials such as epoxy resin can use the simplified model to a high level of approximation, in the experiment we present here, the sample material is acrylic, whose photoelastic response fits the simplified model only with difficulty.

Acrylic in general contains large residual stresses frozen into the material during the manufacturing process. Thus, its photoelastic response to an applied stress will be a linear superposition of both the frozen-stress and applied-stress terms.[10] In addition, its plasticity gives the material a "memory", such that after applying stress it may require a substantial relaxation time to return to its original state. Even after relaxation the material might not return to its original state, thus every sequence of measurements must be preceded by a measurement of the material without applied stress in order to obtain a baseline. Additionally, the plasticity of the sample induces a time-dependent photoelastic response: a continuously applied constant stress will induce a steadily changing birefringence in the sample. Thus, the measurements carried out here we performed as quickly as possible to minimize the time-dependence of the material.

During the experiment, we applied steadily increasing linear stresses to the sample, taking data at each step. Each Stokes spectrum obtained thus represents the polarization state of the beam exiting from the sample, averaged across the beam diameter. The current experiment therefore assumes that the material properties are uniform across the beam aperture. Future research will be directed at implementing the channelled spectropolarimetry technique to an imaging system which will obviate the need for this assumption. If we treat the sample as a linear retarder of unknown retardation amplitude and unknown orientation, we can then use the "Photoelastic Law" to derive the differential stress experienced by the sample[11]:

$$\Delta s = \Delta n / C \ , \tag{8}$$

where $\Delta s$ is the differential stress (expressed in units of force per unit area) and $C$ is the stress-optic coefficient for the sample material. Thus, from the birefringence of the sample derived in the previous section, we can either use the known applied stresses to determine the constant $C$ of the sample material, or, if the constant $C$ is already known, use the result as a direct measure of the accuracy of the procedure. In the case of plastics, the optical constant varies greatly from sample to sample (even using the same nominal chemical composition) even if its time dependency is ignored. The results of our experiment, for both the RCSP and CHSP results using the same sample, are shown in Fig.11.

Because of the large residual stresses frozen into our sample, it is natural to expect that the measurement of stress orientation angle $\phi$ will not be a constant with applied stress. Only for large values of applied stress does the residual stress become ignorable, but large stresses are problematic for the simple model applied here. Nevertheless, for a stress applied at roughly horizontal to the optical system (0°), our fitted results showed a stress orientation angle of 3.6°for the RCSP and 8.7°for the CHSP reconstructions. The discrepancy between the two measurements of $\phi$ is directly linked to the artifacts (indicated in Fig.6) in the CHSP reconstruction for circularly polarized light.

The data presented here is only for very low stresses, in which the photoelastic response of the material can be approximated with a constant stress-optic coefficient $C$; with larger stress, the coefficient begins to decrease, which in the birefringence data is seen as a levelling-off towards a constant value. Given the above measurements of photoelastic response, we calculate a stress-optic coefficient for the sample of $1.13 \times 10^{-12}\text{cm}^2/\text{dyne}$.

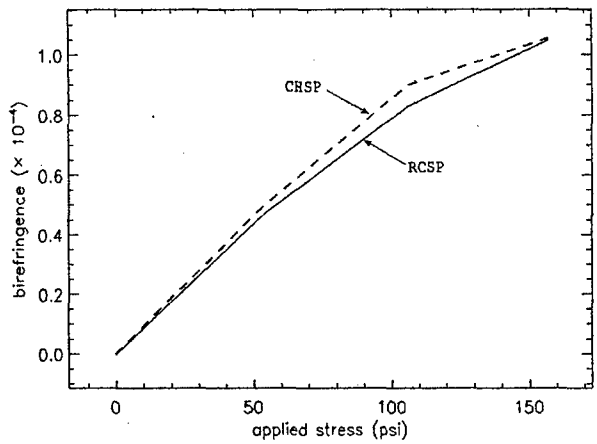


**Figure 11.** The sample birefringence at $\lambda = 550\,\text{nm}$ as a function of applied stress.

## 6. CONCLUSION

The advantages of the channelled spectropolarimetry technique include its simplicity of construction and its minimal use of moving components, which can make it very robust and improve its acquisition speed. The degree of agreement between the RCSP and CHSP instruments shown here indicates the promise of the channelled spectropolarimetry technique, despite the considerable room for improvement in our current instrumentation and reconstruction methodology.

Our lab has for some time now been working on developing novel imaging spectrometer designs, especially for applications which require the measurement of dynamic phenomena. Channelled spectropolarimetry presents obvious advantages for the extension of such a system to polarimetry without some of the difficult issues experienced by other techniques (one example of which would be the co-registration of images in a multiple-detector system). By extension of the photoelasticity experiments shown here to an imaging system, we hope to measure dynamic phenomena such as the propagation of cracks or response to impacts — measurements which can profit from the instrument's ability to simultaneously map the spatial distribution of both stress magnitude and orientation.

## REFERENCES

1. R. M. A. Azzam, "Ellipsometry," in Bass,[12] ch. 27.
2. C. F. Wong, "Birefringence measurement using a photoelastic modulator," *Applied Optics* **18**, pp. 3996–3999, 1979.
3. Q. Zhan and J. R. Leger, "High-resolution imaging ellipsometer," *Applied Optics* **41**, pp. 4443–4450, 2002.
4. R. M. A. Azzam, I. M. Elminyawi, and A. M. El-Saba, "General analysis and optimization of the four-detector photopolarimeter," *J. Opt. Soc. Am. A* **5**(5), pp. 681–689, 1988.
5. K. Oka and T. Kato, "Spectroscopic polarimetry with a channeled spectrum," *Opt. Lett.* **24**(21), pp. 1475–1477, 1999.
6. S. J. Haake and E. A. Patterson, "Photoelastic analysis of frozen stressed specimens using spectral-contents analysis," *Experimental Mechanics* **32**, pp. 266–272, 1992.
7. K. Oka and T. Kato, "Static spectroscopic ellipsometer based on optical frequency-domain interferometry," in *Polarization Analysis, Measurement, and Remote Sensing IV*, pp. 137–140, 2001.
8. R. A. Chipman, "Polarimetry," in Bass,[12] ch. 22.
9. D. A. Holmes, "Exact theory of retardation plates," *J. Opt. Soc. Am.* **54**, pp. 1115–1120, 1964.
10. P. Theocaris and E. Gdoutos, *Matrix Theory of Photoelasticity*, Springer-Verlag, Berlin, 1979.
11. M. M. Frocht, *Photoelasticity*, John Wiley, London, 1941.
12. M. Bass, ed., *Handbook of Optics*, McGraw-Hill, New York, 2 ed., 1995.

16160

## OPSEC REVIEW CERTIFICATION

(AR 530-1, Operations Security)

I am aware that there is foreign intelligence interest in open source publications. I have sufficient technical expertise in the subject matter of this paper to make a determination that the net benefit of this public release outweighs any potential damage.

Reviewer: Andrew Clements GS-13 Electrical Engineer

Name Grade Title

Andrew F. Clements 9 July 2003

Signature Date

Description of Information Reviewed:

Title: Compact Methods for Measuring Stress Birefringence

Author/Originator(s): David Sass, Eustace Dereniak

Publication/Presentation/Release Date: July 2003

Purpose of Release: _____

n abstract, summary, or copy of the information reviewed is available for review.

Reviewer's Determination (check one)

✓ 1. Unclassified Unlimited.

2. Unclassified Limited, Dissemination Restrictions IAW _____

3. Classified. Cannot be released, and requires classification and control at the level of _____

Security Office (AMSTA-CM-XS):

Concur/Nonconcur _____ 11 JUL 03

Signature Date

Public Affairs Office (AMSTA-CM-PI):

Concur/Nonconcur _____ 15 JUL 03

Signature Date

STA 7114-E